

## Microstructure and texture characterization of superplastic Al–Mg–Li alloy

Hong-ping LI<sup>1</sup>, Ling-ying YE<sup>1,2</sup>, Pan ZHANG<sup>1,2</sup>, Jue ZHONG<sup>3</sup>, Ming-hui HUANG<sup>3</sup>

1. School of Materials Science and Engineering, Central South University, Changsha 410083, China;

2. Key Laboratory of Nonferrous Materials, Ministry of Education, Central South University, Changsha 410083, China;

3. College of Mechanical and Electrical Engineering, Central South University, Changsha 410083, China

Received 17 October 2013; accepted 23 April 2014

**Abstract:** A novel thermomechanical processing was developed for producing fine grained Al–Mg–Li alloy sheets. The influences of static recrystallization annealing on the grain structure and superplastic behavior were investigated. The results show that the refined microstructure has a variation in the distribution of grain size, shape and texture across the normal direction of the sheet. The surface layer (SL) has fine, nearly equiaxed grains with a rotated cube<sub>ND</sub> {001}<310> orientation, whereas the center layer (CL) has coarse, elongated grains with a portion of  $\alpha$  fiber orientation. Increasing static recrystallized temperature results in grain growth in the full thickness, decreasing of grain aspect ratio in the center layer, texture sharpening in the surface layer, but weakening in the center layer as well as decreasing of superplastic elongation. Increasing the annealing temperature also produces a sharpening of the rotated cube {001}<310> component and a decreasing of the  $\alpha$  fiber texture in the full thickness of the sheet. The formation mechanisms of recrystallization texture at various temperatures and layers were discussed.

**Key words:** 5A90 Al–Li alloy; thermomechanical processing; texture; superplasticity; recrystallization

### 1 Introduction

Currently, there is a great interest in developing ultra-fine, fully recrystallized grain structure in Al–Mg–Li alloys for superplasticity [1–3]. Moreover, these alloys with ultra-fine recrystallized grains show high service properties and enhanced workability. In contrast, these alloys show poor toughness and limited plasticity at room temperature due to the extensive localization of plastic deformation in the unrecrystallized condition [4]. It is known that the grain size of aluminum alloy can be significantly reduced by severe plastic deformation (SPD) [5,6]. Specifically, fine grains in the order of 0.4–1.6  $\mu\text{m}$  were obtained in Al–Mg–Li alloy by equal-channel angular (ECA) pressing [1,3]. Elongations of up to ~550 % and ~750 % were achieved in the ECA-pressed and high-pressure torsion processed Al–Mg–Li alloy, respectively [7,8]. But, there is a significant disadvantage that the SPD methods are hard to produce fine-grained alloys cost-effectively at a large

scale in comparison with traditional thermomechanical processing (TMP) [9]. TMP uses overaging to develop large precipitates (~1  $\mu\text{m}$ ), and subsequent rolling to form deformation zones around these precipitates. Then fine-grained microstructures can be achieved by particle stimulated nucleation during the following recrystallization annealing. However, it is hard to use TMP consisting of cold or warm rolling to produce fine-grained Al–Mg–Li alloy sheets because of their poor workability at low temperatures that leads to a premature fracture under working conditions [4]. Fortunately, a unique rolling method which used a high starting rolling temperature and a cross-rolling successfully prevented cracking of the sheets, and simultaneously fine grain structure of about 7  $\mu\text{m}$  was achieved by exploiting this rolling method in a new TMP [10,11]. The recrystallization temperature and time, which is the last step of the TMP, influence the grain size, shape and texture, as well as the superplastic behavior of the sheets [12]. The aim of this work is to produce a microstructure that can exhibit superplasticity; attentions

will be focused on the influences of different recrystallization annealing on the grain structures and the superplastic behavior of an Al–Mg–Li alloy 5A90 sheet.

## 2 Experimental

The present study was carried out on a 8.2 mm thick hot rolled Al–Mg–Li alloy 5A90 plate with chemical composition Al–5.2%Mg–2.1%Li–0.12%Zr (mass fraction, %). The plates were first solution treated at 475 °C for 2 h, quenched in water and then overaged at (300 °C, 48 h) + (400 °C, 4 h), subsequently deformed by a two-step rolling with 10%–20% reduction per pass and a rolling speed of about 0.427 m/s as follows.

1) The overaged plates were preheated at 400 °C for 1 h, and then rolled to a reduction of 55% along the rolling direction (RD) of the hot rolled plate.

2) Next, the plates were reheated at 340–380 °C for 1 h, then rolled to the final thickness of about 1.6 mm with reduction of 57% in thickness along the transverse direction (TD) of the hot-rolled plate.

Finally, the rolled sheets were recrystallized at 450–540 °C for 2–60 min in a molten salt bath, then quenched in water. Following TMP, tensile samples were machined parallel to the final rolling direction with a gauge length of 10 mm and a gauge width of 6 mm. Tensile tests were performed at an initial strain rate of  $1 \times 10^{-3} \text{ s}^{-1}$  and a temperature of 525 °C, which was determined to be the optimum conditions for superplastic deformation of this alloy [10,11]. A computer controlled MTS 810 testing machine equipped with a three-zone split furnace was used. The temperature accuracy was within  $\pm 1$  °C. Tensile samples were held about 20 min before deformation. Specimens for optical metallography were annealed at 150 °C for 13 h in order to decorate grain boundaries with second phase particles, then mechanically polished and etched by a special etching solution (1% HF + 4% HCl + 4% HNO<sub>3</sub> + 15% H<sub>2</sub>O (volume fraction, %)) and analyzed on an XJP-6A optical microscope. The average grain sizes in the rolling direction ( $d_{RD}$ ), transverse direction ( $d_{TD}$ ) and normal direction ( $d_{ND}$ ) were measured. Measurements revealed that the rolling direction grain size is approximately equal to the transverse direction grain size ( $d_{RD} \approx d_{TD}$ ). By taking advantage of the approximate equality of  $d_{RD}$  and  $d_{TD}$ , three-dimensional average grain size ( $d_{AVR}$ ) was calculated according to  $d_{AVR} = (d_{RD} \times d_{RD} \times d_{ND})^{1/3}$ . In order to analyze the through-thickness texture variation, texture measurements were performed at a 1/6 thickness of the whole sheet to represent the texture in the surface layer (SL) and a midthickness of the whole sheet to represent the texture in the center layer (CL), respectively. The (111), (200), (220) and (311) pole figures were measured up to a maximum tilt angle of 75°

by the Schulz back-reflection method, using a Bruker D8 Discover X-ray diffractometer. The orientation distribution functions (ODFs) were calculated from the incomplete pole figures after background corrections of the experimental raw pole figures using the series expansion method ( $l_{\max} = 22$ ).

## 3 Results and discussion

### 3.1 Gradient distribution of grain structure and texture

It is known that there usually exists obvious inhomogeneous distribution of recrystallized grain structures along the thickness of Al–Mg–Li alloy 5A90 sheet after TMP [13]. The grain structure can be divided into three layers along the normal direction of the sheet. The two surface layers (SL) contain fine, relatively equiaxed grains, whereas the central layer (CL) contains coarse, elongated grains. The three-dimensional grain structure produced by TMP (recrystallized at 480 °C for 30 min), shown in Fig. 1(a), exhibited an average grain diameter of 5.5  $\mu\text{m}$  and 7.6  $\mu\text{m}$  along the rolling direction for the SL and CL, respectively. The proportion of CL, defined as the ratio of the thickness of CL to that of the whole sheet, was about 1/5. The grain structure of the unprocessed material (solution treated) is shown in Fig. 1(b) for comparison. The statistics for grain sizes produced by TMP and solution treatment are shown in Table 1.

Macrotexture analysis indicated a weak texture for the sheet produced by TMP (recrystallized at 480 °C for 30 min). This is suggested to be a result of particle stimulated nucleation of recrystallization (PSN) [12]. Two ODFs from a 1/6 thickness and a midthickness which represent the texture in SL and CL, respectively, are shown in Fig. 2. While the overall texture is weak, comparison of these two ODFs reveals that there is a distinct texture gradient along the normal direction of the sheet. The SL contains a rotated cube<sub>ND</sub> {001}⟨310⟩ component whereas the CL contains a retention of a portion of  $\alpha$  fiber. For the CL the maximum intensity is found at  $\varphi_1 = 45^\circ$ , which is  $10^\circ$  deviate from the standard position of Brass orientation which is at  $(\varphi_1, \Phi, \varphi_2) = (35^\circ, 45^\circ, 0^\circ)$ . This is suggested to be a result of cross-rolling [14].

### 3.2 Effect of recrystallization annealing on grain structure and texture

The influence of recrystallization temperature and time on the grain size of the sheet after rolling was further investigated. Variation in recrystallization temperature was shown to have less effect on the recrystallized grain size when the alloy was annealed below 510 °C than that at 540 °C. Typical recrystallized

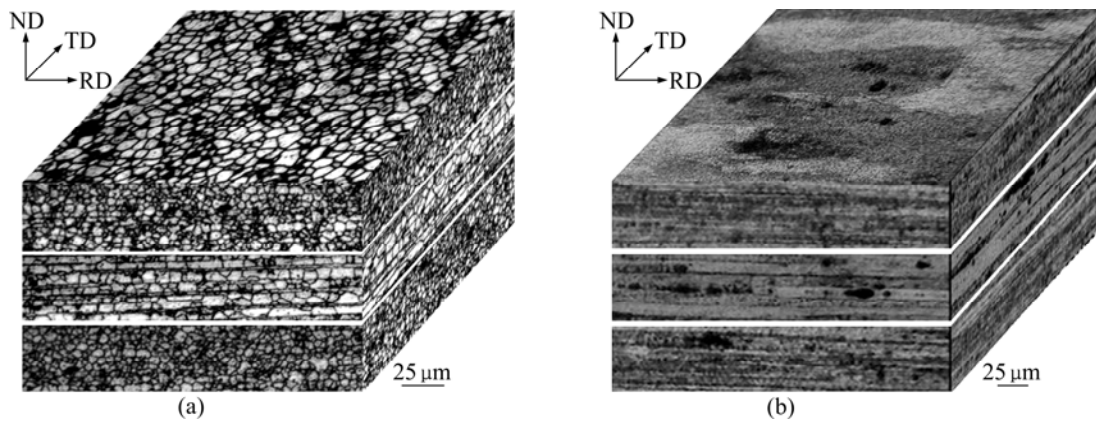


**Fig. 1** Three-dimensional grain structures produced by TMP (recrystallized at 480 °C for 30 min) (a) and unprocessed material, following solution heat treatment for comparison (b)

**Table 1** Grain sizes of material produced by TMP (recrystallized at 480 °C for 30 min) and solution treated (ST) at 475 °C for 2 h

Process	Surface layer			Center layer			Proportion of CL
	$d_{RD}/\mu\text{m}$	$d_{ND}/\mu\text{m}$	GAR	$d_{RD}/\mu\text{m}$	$d_{ND}/\mu\text{m}$	GAR	
TMP	5.5	4.6	1.20	7.6	4.7	1.62	1/5
ST	400	5	80	400	20	20	1/3

GAR is the average grain aspect ratio

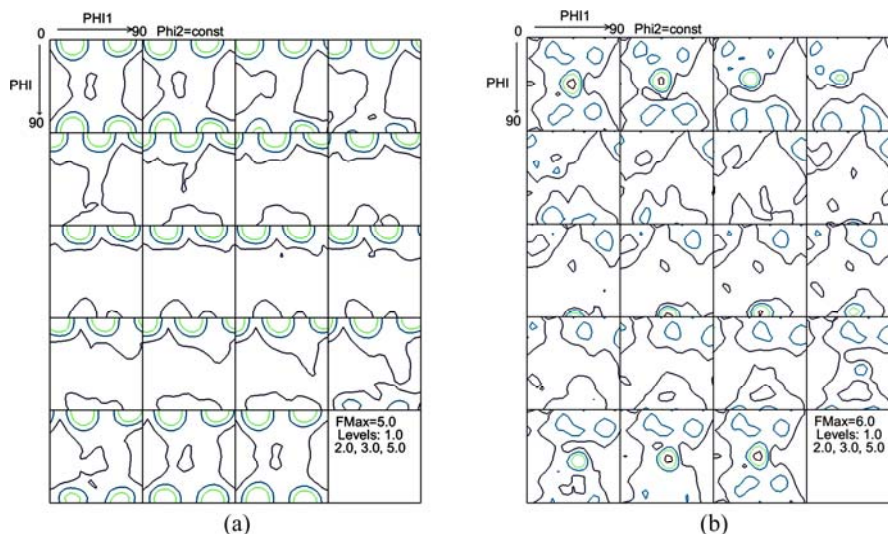


**Fig. 2** ODFs for material followed by TMP (recrystallized at 480 °C for 30 min): (a) Surface layer; (b) Center layer

grain structures in SL are shown in Figs. 3(a) and (b) for the alloy annealed at 450 °C and 540 °C for 1 h, respectively. The average grain size along the rolling direction increased from 4.7 μm to 6.8 μm when the recrystallized temperature was raised from 450 °C to 510 °C; a drastic grain growth happened when the alloy was annealed at 540 °C. In the CL, the grain size had a similar growth trend as that in the SL. Typical grain structures in the CL are shown in Fig. 4 for the alloy annealed at different temperatures for 1 h. It is noted that the elongated grains in the CL gradually transformed to nearly equiaxed grains with the increasing annealing temperature. It is evident that the grain aspect ratio

decreased from 1.60 to 1.20 in the CL whereas that in the SL was almost not changed. The details of the variation of grain size with the recrystallized temperature are shown in Table 2. The three-dimensional average grain size was about 4.6 μm, 5.4 μm, 6.3 μm, 9.6 μm in the SL and 6.2 μm, 6.9 μm, 8.3 μm, 10.4 μm in the CL, respectively, for the alloys annealed at 450 °C, 480 °C, 510 °C, 540 °C for 1 h. Figures 5 and 6 show the variation of texture with the recrystallization temperature in the SL and CL, respectively. In general, texture in these two layers exhibited different trend of variation in texture intensity but same trend of variation in texture components with temperature. In SL, the maximum

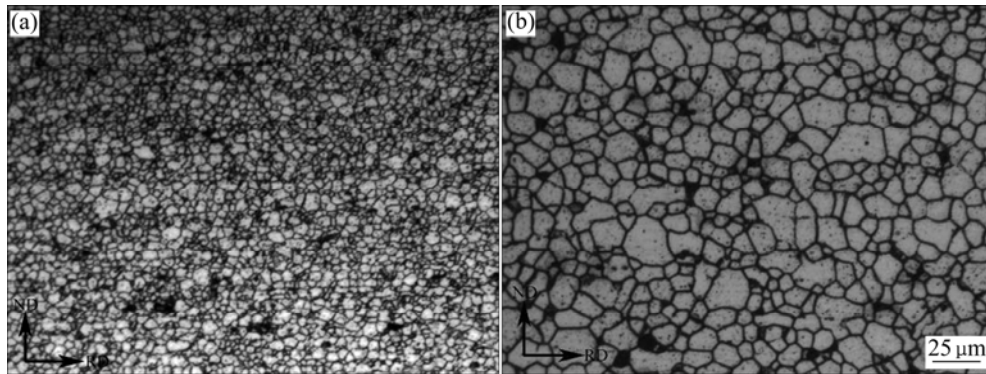


**Fig. 3** Grain structures in surface layer of alloy produced by recrystallization at different temperatures for 1 h after rolling: (a) 450 °C; (b) 540 °C

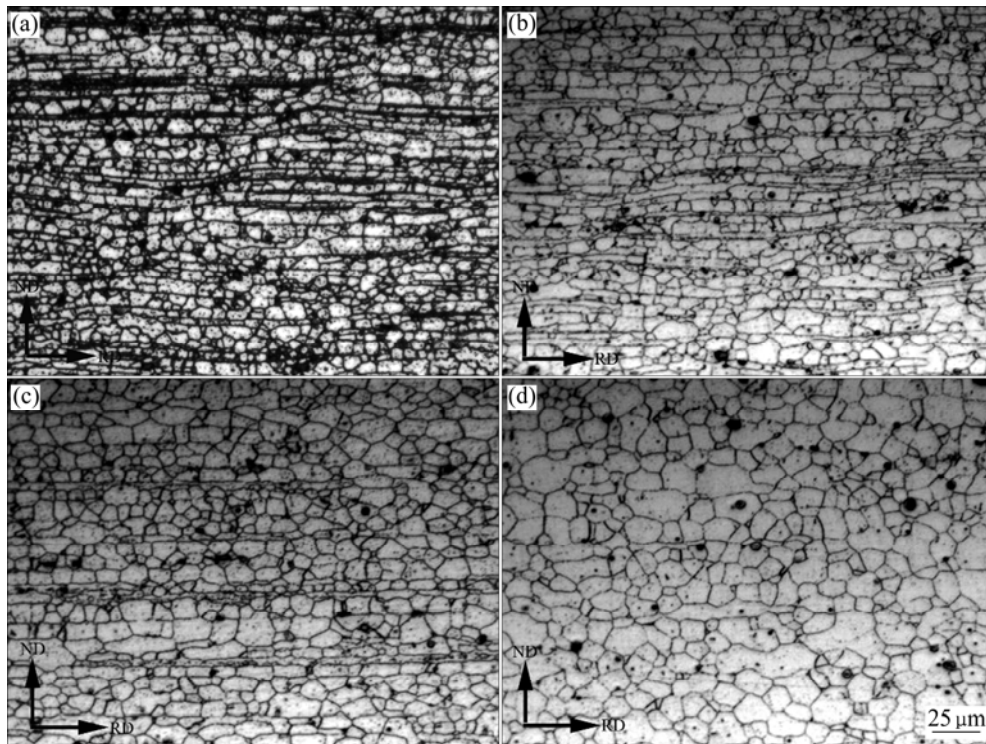


**Fig. 4** Grain structures in center layer of alloy produced by recrystallization at different temperatures for 1 h after rolling: (a) 450 °C; (b) 480 °C; (c) 510 °C; (d) 540 °C

**Table 2** Grain sizes for material followed by rolling and static recrystallization at different temperatures for 1 h

Recrystallization temperature/°C	Surface layer			Center layer		
	$d_{RD}/\mu\text{m}$	$d_{ND}/\mu\text{m}$	GAR	$d_{RD}/\mu\text{m}$	$d_{ND}/\mu\text{m}$	GAR
450	4.7	4.1	1.15	7.2	4.5	1.60
480	5.7	4.8	1.19	8.1	4.9	1.65
510	6.8	5.5	1.24	9.5	6.3	1.51
540	10.1	8.8	1.15	11.1	9.2	1.20

texture intensity increased continuously from 3.88 to 8.18 with the recrystallization temperature increasing from 450 °C to 540 °C, whereas the trend was reversed in the CL where it decreased from 9.95 to 3.78. When it comes to the texture components, after being

recrystallized at 450 °C for 1 h, the texture in SL was a major rotated  $\text{cube}_{ND}\{001\}\langle 310\rangle$  orientation with a mixture of a minor portion of  $\alpha$  fiber orientation. With increasing recrystallization temperature, the rotated  $\text{cube}_{ND}\{001\}\langle 310\rangle$  texture sharpened continuously

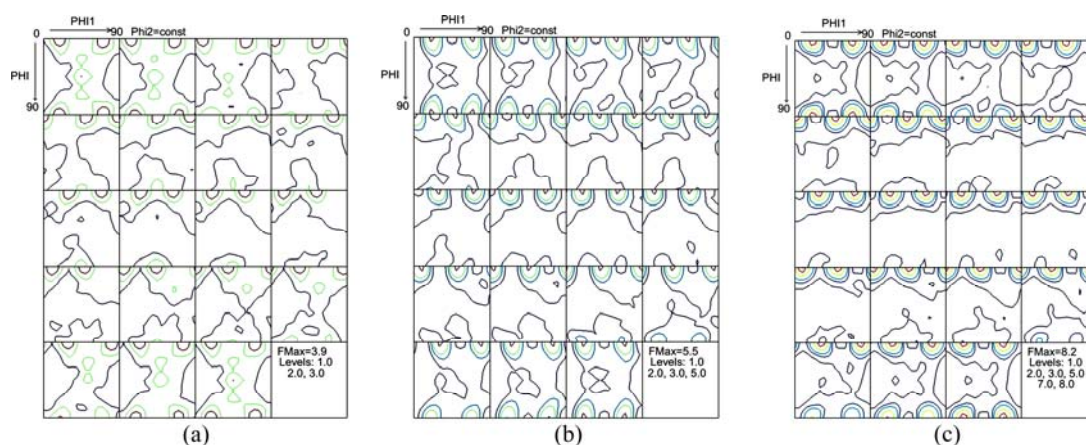


Fig. 5 ODFs for surface layer of alloy after recrystallization at different temperatures for 1 h: (a) 450 °C; (b) 510 °C ; (c) 540 °C

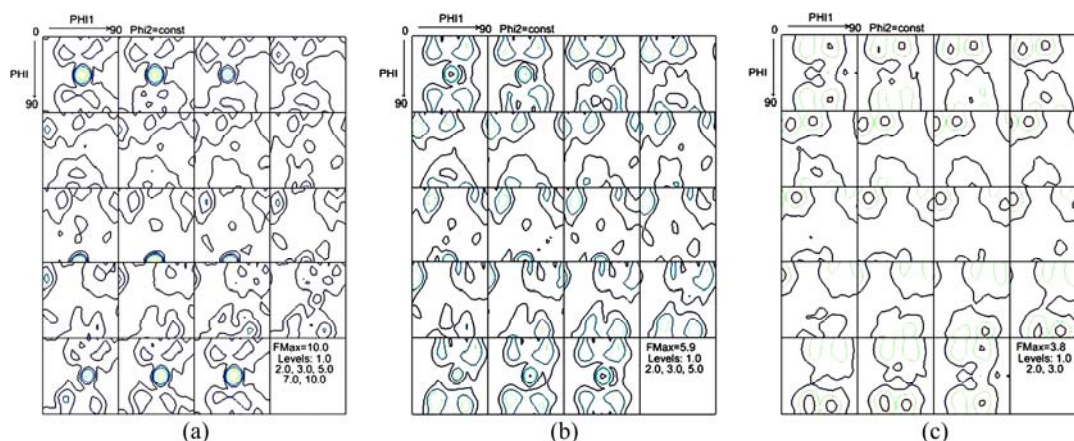


Fig. 6 ODFs for center layer of alloy after recrystallization at different temperatures for 1 h: (a) 450 °C; (b) 510 °C; (c) 540 °C

whereas the  $\alpha$  fiber texture disappeared when the recrystallization temperature increased to 480 °C and above. In the CL, the texture was a major  $\alpha$  fiber orientation when the specimen was recrystallized at 450 °C for 1 h. With increasing the recrystallization temperature, the  $\alpha$  fiber texture weakened continuously and almost disappeared at 540 °C. In contrast, the weak cube<sub>ND</sub> {001}<310> orientation appeared when the alloy was recrystallized at 510 °C and above. So, it can be concluded that, in both cases, increasing the annealing temperature resulted in an sharpening of the rotated cube {001}<310> component and a decreasing of the  $\alpha$  fiber texture.

It is well accepted that recrystallization texture will be weak if the PSN is the nucleation mechanism [12]. This weak texture usually contains a rotated cube<sub>ND</sub> {001}<310> component which is indicative of the nucleation of recrystallization at particles and a retention of rolling texture [15]. ØRSUND and NES [16] developed a model for mechanisms of recrystallization texture formation when materials were experiencing PSN based on the experimental results in a 3xxx aluminum alloy. In their model the type of recrystallization texture

depended on the places at which the new grains nucleated. The deformation zone around the particles contained a gradient of subgrain orientations and dislocation densities which vary with the distance from the particle. If the nucleus initiated at the edge of the deformation zone, where the local degree of misorientation is small, and grew towards the particle, the resultant grain will have an orientation closely linked to the rolling texture. If the nucleus originated at the core of the deformation zone where the local misorientation is most intense, the nucleus and resultant grain will have an orientation distinctly different from that of the deformed matrix. In this case, the recrystallization texture is nearly random, given a uniform particle distribution. This model also showed that a texture transition from rolling texture at low temperatures to a random texture at higher temperatures. In the present study, at the lowest annealing temperature of 450 °C, the result was rather a random texture, suggesting that all the temperatures employed in the present study were higher than the transition temperature. So it can be concluded that the retention of rolling texture in the CL of the sheet is not due to the nucleus initiated at the edge of the

deformation zone.

Indeed, it is known that the presence of small particles will also influence the type of recrystallization texture. If the grain boundary motion is inhibited very effectively by the small precipitates, the retention of rolling texture can be obtained [15]. Before recrystallization during TMP, the Al–Mg–Li alloy 5A90 usually contains a large number of small *S*-phase ( $\text{Al}_2\text{MgLi}$ ) particles, which is produced either by overaging process or by cracking of large *S*-phase during rolling, and do not completely dissolve up to 500 °C [13]. And, the distribution of these small particles is inhomogeneous through the thickness of the sheet. The SL contains a uniform distribution of small particles whereas the CL contains a banded distribution of them. Small particles of  $\beta'$ ( $\text{Al}_3\text{Zr}$ ) which were not dissolved at 530 °C were also present in the Al–Mg–Li alloy 5A90 [17]. It is known that these small particles could prevent grain from growth and they may also suppress PSN due to their drag force on recrystallization nuclei [12]. With increasing the recrystallization temperature, the small *S*-phase particles should start to dissolve, which leads to a decrease in suppression for PSN and a decrease pinning for motion of grain boundaries. Thus the rotated cube<sub>ND</sub> {001}<310> orientation which was a result of nucleation of recrystallization at particles might be strengthened continuously in SL due to the decreasing suppression for PSN, and a drastic grain growth occurred when the annealing temperature was increased to 540 °C at which the *S*-phase ( $\text{Al}_2\text{MgLi}$ ) particles were completely

dissolved. In the CL, when the alloy was annealed at low temperatures, the banded distribution of small particles along rolling direction strongly inhibited the motion of grain boundary along the normal direction of the sheet. So the elongated grain structure was obtained. And, in some regions of CL, grain boundary motion may be completely suppressed and only dislocation motion can take place, which can be evident by the very fine elongated grains among the CL (Fig. 4(a)). Under this condition each volume element of the matrix would become a nucleus of the same orientation as that of the volume element, so that the rolling texture was retained. But, the dissolution of these small precipitates with increasing annealing temperature permitted the growth of grains along the normal direction, which resulted in the transition of elongated grains to equiaxed grains and the weakening of the rolling texture in CL (Fig. 6(b)).

Compared with the recrystallization temperature, the soaking time of recrystallization had less effect on the grain growth. A fully recrystallized grain structure was gained when the specimen was recrystallized at 510 °C for only 2 min, as shown in Fig. 7, with a mean grain size of about 5.9  $\mu\text{m}$  and 8.4  $\mu\text{m}$  in rolling direction for SL and CL, respectively. They were increased to 6.8  $\mu\text{m}$  and 9.5  $\mu\text{m}$  upon soaking for 1 h at the same temperature. In addition, the grain aspect ratios were almost not changed for both the SL and CL. The details of the variation of grain size with soaking time at 510 °C are shown in Table 3. Figure 7(b) shows the adjoining area of SL and CL, in which the fine, equiaxed grains

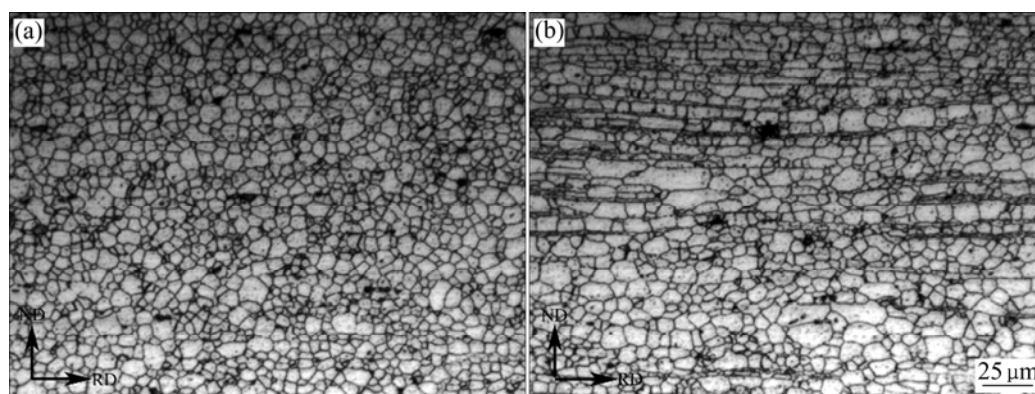


**Fig. 7** Grain structures of alloy produced by recrystallization at 510 °C for 2 min after rolling: (a) Surface layer; (b) Transition area from surface layer to center layer

**Table 3** Grain sizes for material after rolling and static recrystallization at 510 °C for different soaking time

Soaking time at 510 °C/min	Surface layer			Center layer		
	$d_{\text{RD}}/\mu\text{m}$	$d_{\text{ND}}/\mu\text{m}$	GAR	$d_{\text{RD}}/\mu\text{m}$	$d_{\text{ND}}/\mu\text{m}$	GAR
2	5.9	4.9	1.20	8.4	5.1	1.65
10	6.1	5.1	1.18	8.9	5.6	1.57
30	6.3	5.2	1.21	9.1	5.9	1.54
60	6.8	5.5	1.24	9.5	6.3	1.51

gradually changed to elongated grains. The selected area shown in Fig. 7(b) was about 0.7 mm far from the rolling surface and the ratio of the thickness of CL to that of the whole sheet was about 1/5.

### 3.3 Effect of recrystallization annealing on superplastic behavior

Figure 8 shows the superplastic elongations of the alloy 5A90. Figure 9 shows the true stress–true strain curves for the alloy 5A90 recrystallized at different temperatures for 1 h that was deformed at an initial strain rate of  $1 \times 10^{-3} \text{ s}^{-1}$  and a temperature of 525 °C. The elongation decreased from 765% to 600% when the recrystallization temperature raised from 450 °C to 540 °C. The flow stress increased and strain for peak stress decreased with the increase of recrystallization temperature. Similar investigation such as superplastic behavior of AA8090 alloy with gradients in microstructure and texture was done systematically by FAN et al [18]. They found that the texture could result in the difference in flow behavior. However, in the present study, the alloy 5A90 sheet after being recrystallized at

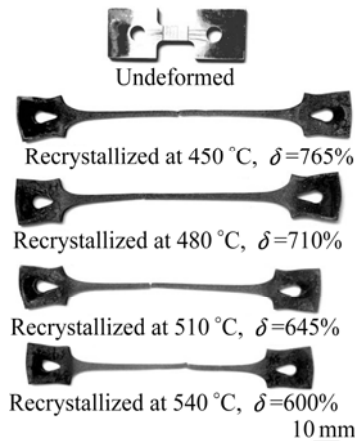


Fig. 8 Effects of recrystallization temperature on superplastic elongation of samples

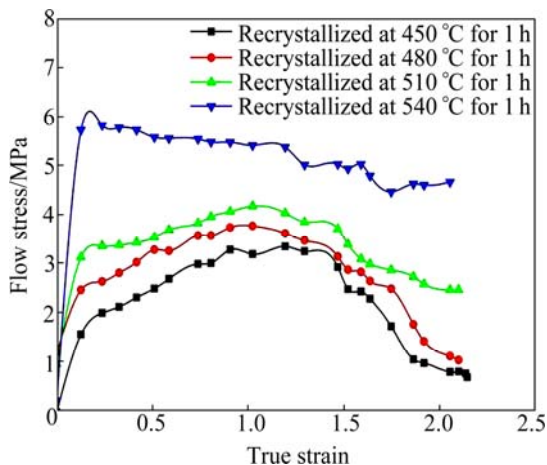


Fig. 9 True stress–strain curves of samples deformed at initial strain rate of  $1 \times 10^{-3} \text{ s}^{-1}$  and 525 °C

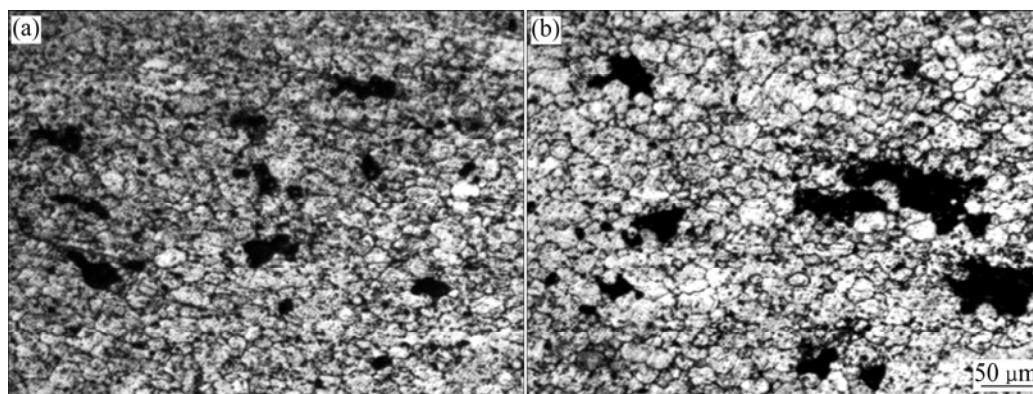
450–540 °C contained a weak texture and the components of texture were similar. So it is suggested that the difference in flow behavior in Fig. 9 was not ascribed to the texture but to the difference in initial grain size. From Fig. 9 two types of stress–strain curves can be distinguished. The sheets recrystallized at 450 °C, 480 °C and 510 °C, in which the grain sizes of about 4 to 7  $\mu\text{m}$  were obtained, show similar type of stress–strain curves during superplastic deformation; there is no apparent steady state flow for these three curves, and they can be divided into two parts.

In the first part, the flow stress increases gradually before reaching a peak stress. In the second part, it decreases to failure accompanied by small fluctuations in stress. In contrast, the sheet recrystallized at 540 °C having grain sizes of about 10  $\mu\text{m}$  shows another type of stress–strain curve. Its flow stress increases sharply to peak stress at the initial stage of deformation, then shifts to a nearly steady state flow accompanied by fluctuation in a small range towards the end of deformation. The difference in flow behavior can be explained by the variation in the grain size. Both the static (grip section) and dynamic (gauge section) grain growth were observed during the deformation. The grain sizes observed after static annealing and superplastic deformation, and the grain aspect ratio in the SL are summarized in Table 4. For the samples recrystallized at 450 °C to 510 °C before deformation, the grain sizes in the grip section increased from the initial value of 4.7–6.8  $\mu\text{m}$  to 8.4–9.3  $\mu\text{m}$  after deformation in the SL. However, for the sample recrystallized at 540 °C before deformation, the grain size in the grip section was almost not changed during the deformation in the SL. This suggested that the fine grains formed during recrystallization at 450 °C to 510 °C were not statically stable at the deformation temperature of 525 °C. It was known that the flow stress increased with the increase in grain size, so the flow stress for the samples recrystallized at 450–510 °C increased gradually in the first part of stress–strain curves due to a remarkable increase in grain size. But for the sample recrystallized at 540 °C which was higher than the deformation temperature, its grains were stable and did not grow so significantly as those recrystallized below 510 °C, which resulted in decreasing favorable contribution to flow stress, so the stress–strain curves suggest a near steady state of flow stress.

The typical microstructures in the CL of gauge section (near shoulder), for the samples undergone static recrystallization at 450 °C and 540 °C after deformed to failure, are shown in Fig. 10. From Fig. 10 and Table 4, it can be concluded that superplastic deformation resulted in a much faster grain growth than static annealing. The grain sizes in the gauge section were almost twice that in the grip section. It was also noted that transformation

**Table 4** Grain sizes after static annealing (grip section, numerator) and superplastic deformation (denominator) for material after rolling and static recrystallization for 1 h at different temperatures

Recrystallization temperature/°C	Surface layer			Center layer		
	$d_{RD}/\mu\text{m}$	$d_{ND}/\mu\text{m}$	GAR	$d_{RD}/\mu\text{m}$	$d_{ND}/\mu\text{m}$	GAR
450	8.4/–	6.5/–	1.29/–	10.6/18.1	6.7/13.4	1.58/1.35
480	9.1/–	7.3/–	1.25/–	11.1/18.6	6.8/14.1	1.63/1.32
510	9.3/–	7.5/–	1.24/–	11.4/19.3	7.0/15.2	1.63/1.27
540	10.4/–	8.9/–	1.17/–	12.8/21.2	9.4/15.9	1.36/1.33

**Fig. 10** Typical microstructures in center layer of alloy recrystallized at different temperatures for 1 h deformed to failure at an initial strain rate of  $1 \times 10^{-3} \text{ s}^{-1}$  and 530 °C: (a) 450 °C; (b) 540 °C

from elongated grains to equiaxed grains occurred in the CL during superplastic deformation. It can be seen from Fig. 10 that cavitations have irregular shape and tend to interlink and grow along the tensile direction, and their sizes increase with increasing initial grain sizes before deformation. Since the distribution of cavitations along the gauge is inhomogeneous [19], both the microstructures shown in Fig. 10 were located at the positions 10 mm distance away from the fracture tips.

## 4 Conclusions

1) The refined microstructure after TMP has a variation in distribution of grain size, shape and texture across the normal direction of the sheet. The surface layer has fine, nearly equiaxed grains with a rotated  $\text{cube}_{ND} \{001\} \langle 310 \rangle$  texture, whereas the center layer has coarse, elongated grains with a portion of  $\alpha$  fiber texture. The three-dimensional average grain size is about  $4.6 \mu\text{m}$  in the surface layer and  $6.2 \mu\text{m}$  in the center layer, respectively, after being annealed at 450 °C for 1 h.

2) Variation in recrystallization temperature has less effect on the recrystallized grain size when the alloy is annealed below 510 °C than at 540 °C. Especially, increasing static recrystallization temperature from 450 °C to 510 °C and from 510 °C to 540 °C results in a grain growth by  $2.1 \mu\text{m}$  and  $3.3 \mu\text{m}$  in rolling direction of surface layer, respectively.

3) The maximum elongation obtained is 765% in

the (450 °C, 1 h) recrystallized material when it was deformed at 525 °C with strain rate  $1 \times 10^{-3} \text{ s}^{-1}$ . The elongation decreases with the increase in static recrystallization temperature, which is attributed to grain growth.

## References

- [1] FURUKAWA M, BERBON P, LANGDON T G, HORITA Z, NEMOTO M, TSENEV N, VALIEV R. Age hardening and the potential for superplasticity in a fine-grained Al–Mg–Li–Zr alloy [J]. *Metallurgical and Materials Transactions A*, 1998, 29(1): 169–177.
- [2] FURUKAWA M, IWAHASHI Y, HORITA Z, NEMOTO M, TSENEV N K, VALIEV R Z, LANGDON T G. Structural evolution and the Hall-Petch relationship in an Al–Mg–Li–Zr alloy with ultra-fine grain size [J]. *Acta Materialia*, 1997, 45(11): 4751–4757.
- [3] MAZILKIN A A, MYSHLYAEV M M. Microstructure and thermal stability of superplastic aluminium–lithium alloy after severe plastic deformation [J]. *Journal of Materials Science*, 2006, 41(12): 3767–3772.
- [4] KAIBYSHEV R, SHIPILOVA K, MUSIN F, MOTOHASHI Y. Achieving high strain rate superplasticity in an Al–Li–Mg alloy through equal channel angular extrusion [J]. *Materials Science and Technology*, 2005, 21(4): 408–418.
- [5] JIANG Jing-hua, MA Ai-bin, SAITO N, WATAZU A, LIN Ping-hua, NISHIDA Y. Effect of microstructures on superplasticity of Al–11%Si alloy [J]. *Transactions of Nonferrous Metals Society of China*, 2007, 17(3): 509–513.
- [6] LIU Man-ping, SUN Shao-chun, ROVEN H J, YU Ying-da, ZHANG Zhen, MURASHKIN M, VALIEV R Z. Deformation defects and electron irradiation effect in nanostructured Al–Mg alloy processed by severe plastic deformation [J]. *Transactions of Nonferrous Metals Society of China*, 2012, 22(8): 1810–1816.

- [7] VALIEV R Z, ISLAMGALIEV R K, STOLYAROV V V, MISHRA R S, MUKHERJEE A K. Processing and mechanical properties of nanocrystalline alloys prepared by severe plastic deformation [J]. Materials Science Forum, 1998, 269–272: 969–974.
- [8] MISHRA R S, VALIEV R Z, MCFADDEN S X, ISLAMGALIEV R K, MUKHERJEE A K. High-strain-rate superplasticity from nanocrystalline Al alloy 1420 at low temperature [J]. Philosophical Magazine A, 2001, 81(1): 37–48.
- [9] HUMPHREYS F J, PRANGNELL P B, PRIESTNER R. Fine-grained alloys by thermomechanical processing [J]. Current Opinion in Solid State and Materials Science, 2001, 5(1): 15–21.
- [10] YE L Y, ZHANG X M, ZHENG D W, LIU S D, TANG J G. Superplastic behavior of an Al–Mg–Li alloy [J]. Journal of Alloys and Compounds, 2009, 487(1–2): 109–115.
- [11] ZHANG X M, YE L Y, LIU Y W, TANG J G, ZHENG D W. Superplasticity of an Al–Mg–Li alloy prepared by thermomechanical processing [J]. Materials Science and Technology, 2011, 27(10): 1588–1592.
- [12] HUMPHREYS F J, HATHERLY M. Recrystallization and related annealing phenomena [M]. 2nd ed. Oxford: Pergamon Press, 2004.
- [13] ZHANG Xing-ming, YE Ling-ying, LIU Ying-wei, DU Yu-xuan, LUO Zhi-huo. The formation mechanism of gradient-distributed particles and their effects on grain structure in 01420 Al–Li alloy [J]. Journal of Central South University of Technology, 2008, 15(2): 147–152.
- [14] HUH M Y, CHO S Y, ENGLER O. Randomization of the annealing texture in aluminum 5182 sheet by cross-rolling [J]. Materials Science and Engineering A, 2001, 315(1): 35–46.
- [15] ENGLER O, LÜCKE K. Mechanisms of recrystallization texture formation in aluminium alloys [J]. Scripta Metallurgica, 1992, 27(11): 1527–1532.
- [16] ØRSUND R, NES E. A model for the nucleation of recrystallization from particles: The texture aspect [J]. Scripta Metallurgica, 1988, 22(5): 671–676.
- [17] FRIDLANDER J N, KOLOBNEV N I, KHOKHLATOVA L B, SEMENOVA H Y. Peculiarities of structural formation in 1420 alloy sheets [J]. Aluminium, 1992, 68(4): 334–336.
- [18] FAN W, KASHYAP B P, CHATURVEDI M C. Anisotropy in flow and microstructural evolution during superplastic deformation of a layered-microstructured AA 8090 Al–Li alloy [J]. Materials Science and Engineering A, 2003, 349(2): 166–182.
- [19] ZHAO Sha, YE Ling-ying, ZHANG Xing-ming. Inhomogeneity of 5A90 Al–Li alloy during superplastic deformation and its effect on evolution of cavity [J]. The Chinese Journal of Nonferrous Metals, 2013, 23(8): 2125–2132. (in Chinese)

## 超塑 Al–Mg–Li 合金的显微组织与织构特性

李红萍<sup>1</sup>, 叶凌英<sup>1,2</sup>, 张盼<sup>1,2</sup>, 钟掘<sup>3</sup>, 黄明辉<sup>3</sup>

1. 中南大学 材料科学与工程学院, 长沙 410083;

2. 中南大学 教育部有色金属材料科学与工程教育部重点实验室, 长沙 410083;

3. 中南大学 机电工程学院, 长沙 410083

**摘要:** 采用一种新型形变热处理方法制备细晶 Al–Mg–Li 合金板材, 研究静态再结晶退火对合金板材晶粒组织及超塑变形行为的影响。结果表明, 晶粒尺寸、形状和织构的分布沿板材法向方向存在明显不同; 表面层的晶粒组织细小、等轴, 含有旋转  $\text{cube}_{\text{ND}}\{001\}\langle 310\rangle$  取向; 中心层具有粗大、长条状晶粒, 含有  $\alpha$  取向线的织构组分。随着再结晶温度的升高, 整个板材的晶粒尺寸长大, 中心层晶粒纵横比减小, 表面层织构强化而中心层织构弱化, 超塑性伸长率下降。升高再结晶温度导致整个板材内的旋转  $\text{cube}_{\text{ND}}\{001\}\langle 310\rangle$  织构组分强化而  $\alpha$  取向线的织构弱化。分析了不同温度下再结晶织构的形成机制。

**关键词:** 5A90 铝锂合金; 形变热处理; 织构; 超塑性; 再结晶

(Edited by Sai-qian YUAN)